Anisotropic grid-based formulas for subgrid-scale models

By G.-H. Cottet[1] AND A. A. Wray

1. Motivations and objectives

Anisotropic subgrid-scale models have long been recognized as a natural alternative to the isotropic Smagorinsky model. *A priori* tests, based either on experiments (Liu *et al.* 1994) or on DNS data have often shown that these models have much better correlations than the Smagorinsky model. However their efficacy in large eddy simulations has so far been limited by two factors. First, these models are in general viewed, through Taylor expansions, as a way to compute the subgrid-scale contribution of the Leonard term. They are used with the coefficient values which result from these Taylor expansions and thus depend on the form of the filter function. Secondly, anisotropic models are based on tensor forms of the turbulent viscosity and therefore may produce backscatter as well as dissipation. The clipping techniques, which are proposed (Liu *et al.* 1994, Vreman *et al.* 1997) to overcome the destabilizing effects of backscatter, are based on energy balances but ignore that dissipation and backscatter in general coexist at every point along different strain directions of the flow. They thus lead to models which are not dissipative enough, which explains why they are often complemented by Smagorinsky terms in so-called *mixed* models. These formulations, however, are not able to retain the potential gain offered by the anisotropy of the original model, in particular in laminar or wall-bounded flows.

Our goal here is twofold. We first derive formulas based on the quantities computed on the grid that facilitate the implementation of the anistropic model in any code. By distinguishing between backscatter and dissipation directions in the flow, we also present strictly dissipative formulas which lead to stable and truly anisotropic schemes.

2. Accomplishments

2.1 The model

Our starting point will be the following model for the residual shear stresses, sometimes referred to as the self-similarity model (Liu *et al.* 1994) or the gradient model (Vreman *et al.* 1997):

$$\tau_{ij} \simeq C\Delta^2 D_{ik}\overline{\mathbf{u}} D_{jk}\overline{\mathbf{u}} \tag{1}$$

where $D_{ik}\overline{\mathbf{u}} = \frac{\partial \overline{u}_i}{\partial x_k}$ and Δ is the filter width. Throughout the paper, we will use the convention of summation of repeated indices.

1 Permanent address: LMC-IMAG, Université Joseph Fourier, BP 53 Grenoble Cédex 9, France

2.1.1 Integral approximation and grid formulas

Our derivation is based on a numerical filter function ζ satisfying the following moment conditions:

$$\int x_k x_l \zeta(\mathbf{x})\, d\mathbf{x} = \delta_{kl}\ ,\ k,l = 1,2,3 \tag{2}$$

where x_k denote the components of $\mathbf{x}$ and δ_{kl} is the Kronecker symbol. Such a filter can be easily constructed by proper rescaling of any positive function satisfying symmetry properties (e.g. functions with spherical symmetry or functions constructed through tensor product of one-dimensional even functions).

We first write (here and in the sequel we drop the overbar notation for the resolved fields)

$$\Delta^2 D_{ik}\mathbf{u}(\mathbf{x}) D_{jk}\mathbf{u}(\mathbf{x}) = \Delta^{-3} \int D_{ik}\mathbf{u}(\mathbf{x}) D_{jl}\mathbf{u}(\mathbf{x})(y_k - x_k)(y_l - x_l)\zeta(\frac{\mathbf{y}-\mathbf{x}}{\Delta})\, d\mathbf{y} \tag{3}$$

where we recall that the summation of repeated indices is implied. In the above formula, Δ is the filter width, which for the time being is assumed to be constant. By Taylor expansions of u_i and u_j around $\mathbf{x}$, this yields

$$\Delta^2 D_{ik}\mathbf{u}(\mathbf{x}) D_{jk}\mathbf{u}(\mathbf{x}) = \Delta^{-3}\left\{ \int [u_j(\mathbf{y}) - u_j(\mathbf{x})][u_i(\mathbf{y}) - u_i(\mathbf{x})]\zeta(\frac{\mathbf{y}-\mathbf{x}}{\Delta})\, d\mathbf{y} + O(\Delta^2) \right\}. \tag{4}$$

Since ultimately it is the divergence of τ_{ij} that we need to model in order to solve the filtered Navier-Stokes equations, we take the divergence of (4) to obtain, after cancellation of the term involving the divergence of $\mathbf{u}$:

$$\partial_j \left[D_{ik}\mathbf{u}(\mathbf{x}) D_{jk}\mathbf{u}(\mathbf{x}) \right] \simeq A_i + B_i$$

where we used the notation ∂_j for $\partial/\partial x_j$ and

$$A_i = -\Delta^{-3} \int [u_j(\mathbf{y}) - u_j(\mathbf{x})]\partial_j u_i(\mathbf{x})\zeta(\frac{\mathbf{y}-\mathbf{x}}{\Delta})\, dy$$

$$B_i = -\Delta^{-4} \int [u_j(\mathbf{y}) - u_j(\mathbf{x})][u_i(\mathbf{y}) - u_i(\mathbf{x})]\partial_j\zeta(\frac{\mathbf{y}-\mathbf{x}}{\Delta})\, d\mathbf{y}$$

It is readily seen that A_i are convective terms: if one sets $\lambda = \int \zeta(\mathbf{y})\, d\mathbf{y}$ and

$$\hat{\mathbf{u}}(\mathbf{x}) = \frac{1}{\lambda\Delta^3} \int \mathbf{u}(\mathbf{y})\zeta(\frac{\mathbf{y}-\mathbf{x}}{\Delta})\, d\mathbf{y}$$

then A_i can be rewritten as $(\hat{\mathbf{u}} - \mathbf{u})\nabla u_i$. It thus does not contribute to the energy balance. Since the goal of SGS models is to model the transfer of energy between

large and small scales, we will only be interested in B_i. Hence the SGS model can be expressed as

$$\partial_j \tau_{ij} \simeq -C\Delta^{-4} \int [u_j(\mathbf{y}) - u_j(\mathbf{x})][u_i(\mathbf{y}) - u_i(\mathbf{x})] \partial_j \zeta(\frac{\mathbf{y}-\mathbf{x}}{\Delta})\, d\mathbf{y} \tag{5}$$

2.1.2 Viscous scales and grid refinement

The above derivation assumes an isotropic filter ζ. In practice, it is natural to use a function which matches the computational grid. For a variable grid such as those generally used for wall-bounded flows, one can then expect that grid refinement in specific directions will translate into variable viscous length scales in the subgrid-scale model. To be more specific let us assume that the filter ζ is built from a unique one-dimensional shape ρ in all 3 directions and that $\Delta_1(x_1), \Delta_2(x_2), \Delta_3(x_3)$ are the local grid sizes in the 3 directions. The natural generalization of formulas (4) and (5) to this case is given by

$$\tau_{ij}(\mathbf{x}) \simeq \frac{C}{\omega(\mathbf{x})} \int [u_j(\mathbf{y}) - u_j(\mathbf{x})][u_i(\mathbf{y}) - u_i(\mathbf{x})] \zeta(\mathbf{x},\mathbf{y})\, d\mathbf{y}$$

$$\partial_j \tau_{ij}(\mathbf{x}) \simeq \frac{C}{\omega(\mathbf{x})} \frac{1}{\Delta_j(x_j)} \int [u_j(\mathbf{y}) - u_j(\mathbf{x})][u_i(\mathbf{y}) - u_i(\mathbf{x})] \lambda_j(\mathbf{x},\mathbf{y})\, d\mathbf{y}$$

where $\omega(\mathbf{x}) = \Delta_1(x_1)\Delta_2(x_2)\Delta_3(x_3)$ is the volume of the cell centered at $\mathbf{x}$ and

$$\zeta(\mathbf{x},\mathbf{y}) = \rho(\frac{x_1 - y_1}{\Delta_1(\mathbf{x})})\rho(\frac{x_2 - y_2}{\Delta_2(\mathbf{x})})\rho(\frac{x_3 - y_3}{\Delta_3(\mathbf{x})})$$

$$\lambda_1(\mathbf{x},\mathbf{y}) = \rho'(\frac{x_1 - y_1}{\Delta_1(\mathbf{x})})\rho(\frac{x_2 - y_2}{\Delta_2(\mathbf{x})})\rho(\frac{x_3 - y_3}{\Delta_3(\mathbf{x})}).$$

and similar formulas for λ_2, λ_3. It can be shown (see Cottet 1997 for details) by using a coordinate mapping between the mesh and a uniform isotropic grid that these formulas correspond to the differential subgrid-scale model

$$\tau_{ij} \simeq \Delta_k(\mathbf{x})^2 D_{ik}\mathbf{u} D_{jk}\mathbf{u}$$

In other words, the eddy-viscosity length scale is given by the grid spacing in the corresponding direction. In near wall regions, when grid refinement is used, this produces an additional damping in the SGS dissipation which we believe is desirable. Note that the traditional derivation of subgrid-scale models does not apply to varying size filters, making the use of (1) questionable.

2.1.3 Anisotropic clipping

The total subgrid-scale dissipation $\mathcal{D}$ associated to the model (5) is obtained by multiplying this formula by $\mathbf{u}(\mathbf{x})$ and integrating over $\mathbf{x}$. Writing $\mathbf{u}(\mathbf{x}) = \frac{1}{2}[\mathbf{u}(\mathbf{x}) + \mathbf{u}(\mathbf{y})] + \frac{1}{2}[\mathbf{u}(\mathbf{x}) - \mathbf{u}(\mathbf{y})]$ and using the symmetry of ζ, we are left with

$$\mathcal{D} = \frac{C}{2}\Delta^{-4} \int [\mathbf{u}(\mathbf{y}) - \mathbf{u}(\mathbf{x})] \cdot \nabla\zeta(\frac{\mathbf{y}-\mathbf{x}}{\Delta})|\mathbf{u}(\mathbf{y}) - \mathbf{u}(\mathbf{x})|^2\, d\mathbf{x}\, d\mathbf{y}$$

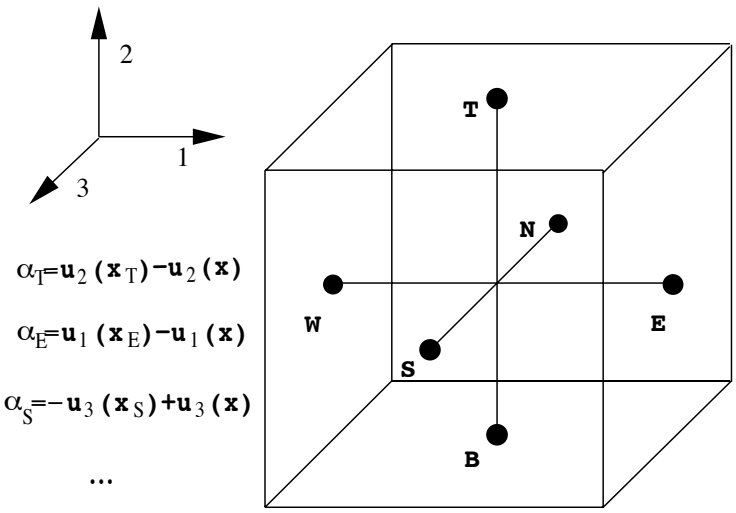

FIGURE 1. Finite-difference stencil of the subgrid-scale model in the case of a uniform grid with a radial hat filter. $\alpha_T/\Delta, \alpha_E/\Delta, \cdots$ denote the weights of the corresponding grid points.

This formula gives a way to measure the local dissipation at a given point $\mathbf{x}$ as well by restricting the integral over $\mathbf{y}$ only. It also enables us to formulate a strictly dissipative model as follows

$$\partial_j \tau_{ij}(\mathbf{x}) \simeq \Delta^{-4} \int \left\{ [\mathbf{u}(\mathbf{x}) - \mathbf{u}(\mathbf{y})] \cdot \nabla \zeta(\frac{\mathbf{x}-\mathbf{y}}{\Delta}) \right\}_+ [\mathbf{u}(\mathbf{x}) - \mathbf{u}(\mathbf{y})]\, d\mathbf{y} \qquad (6)$$

where $a_+ = \max(0, a)$. Unlike the traditional clipping strategies, which would consist in replacing $\partial_j \tau_{ij}$ by zero whenever the global energy budget would have the wrong sign, this technique respects the anisotropy of the original formula in the sense that it allows to dissipate in one or more directions while controlling the backscatter which would arise in the other directions. A clipping technique can be written along the same lines to make sure that when combining the subgrid-scale model with the effect of the molecular viscosity the method is strictly dissipative.

2.2 Large eddy simulations

2.2.1 Isotropic turbulence

We first examine the validity of our model in simulations of decaying isotropic turbulence. All calculations were done with a spectral code in a periodic box with full dealiasing. The subgrid-scale models is therefore implemented on a uniform grid on which velocity values are classically obtained through FFT.

We have considered two possible choices for the numerical filter ζ: a radial function $\zeta_1(\mathbf{x}) = \alpha f(|\mathbf{x}|)$ and a tensor product function $\zeta_2(\mathbf{x}) = \beta f(x_1) f(x_2) f(x_3)$. The function f is a piecewise quadratic spline with support in $[-1.5, +1.5]$, and α, β

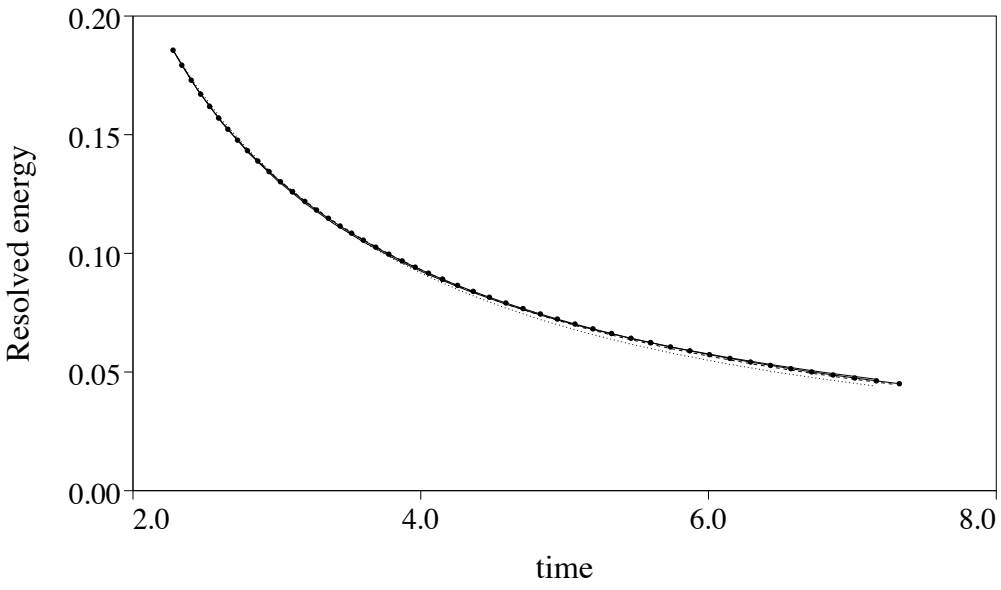

FIGURE 2. Energy decay for DNS and LES with Smagorinsky and anisotropic models. ○ : DNS results ——— : Smagorinsky model ····· : Anisotropic model with 27 points filter ---- : Anisotropic model with 7 points filter.

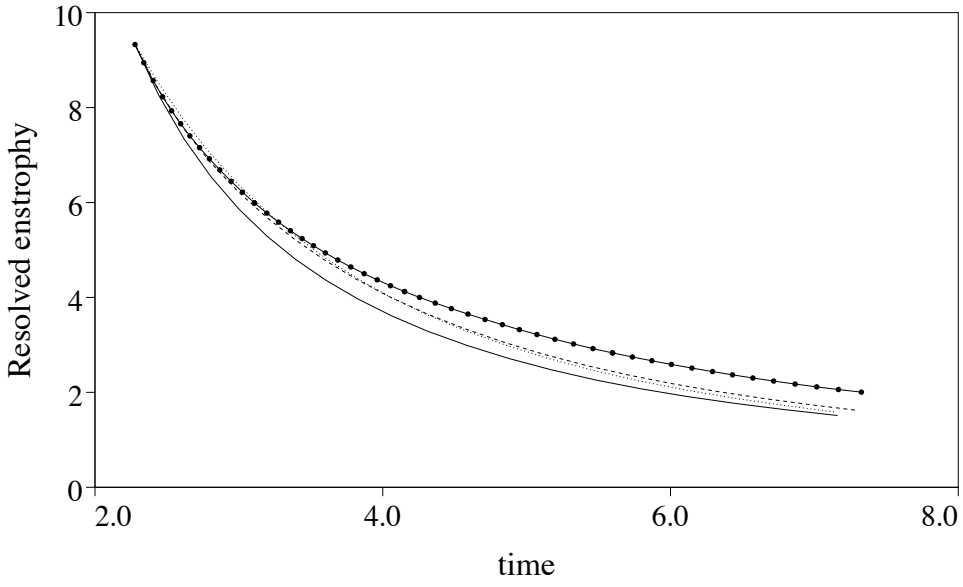

FIGURE 3. Enstrophy decay for DNS and LES with Smagorinsky and anisotropic models. See Fig. 2 for symbol legend.

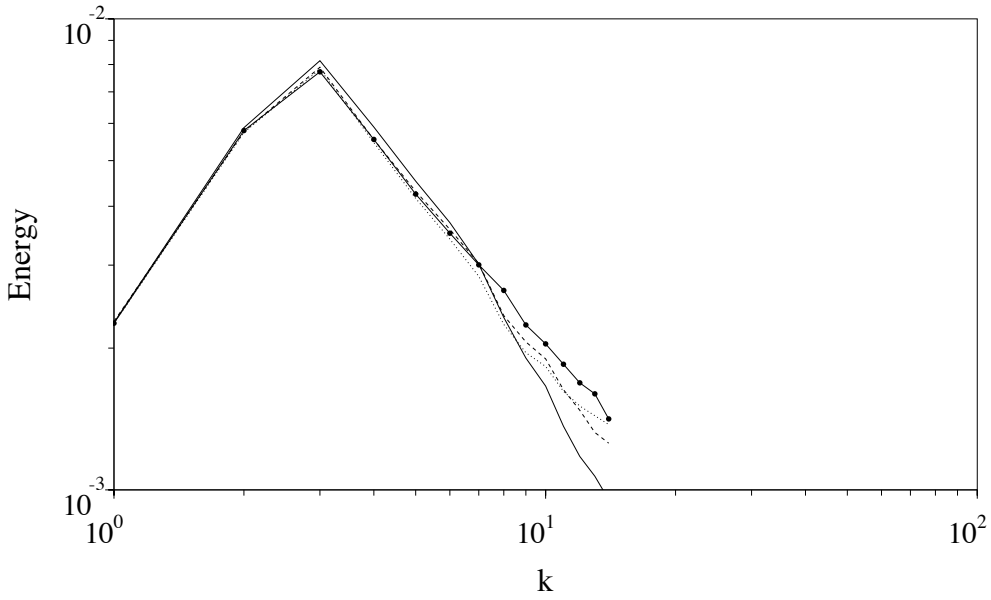

FIGURE 4. Energy spectra at $t = 4.$ for DNS and LES. See Fig. 2 for symbol legend.

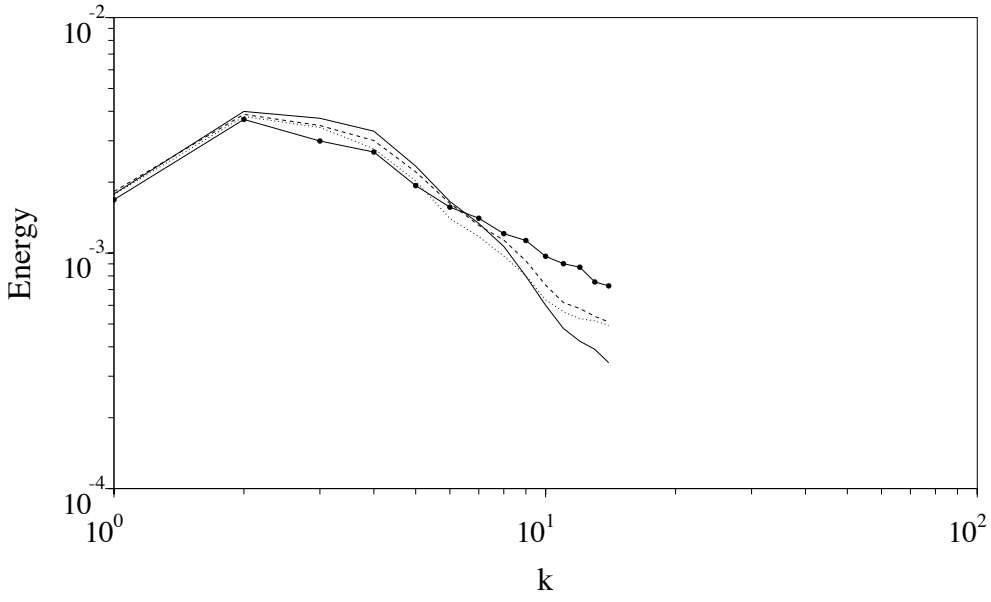

FIGURE 5. Energy spectra at $t = 7.$ See Fig. 2 for symbol legend.

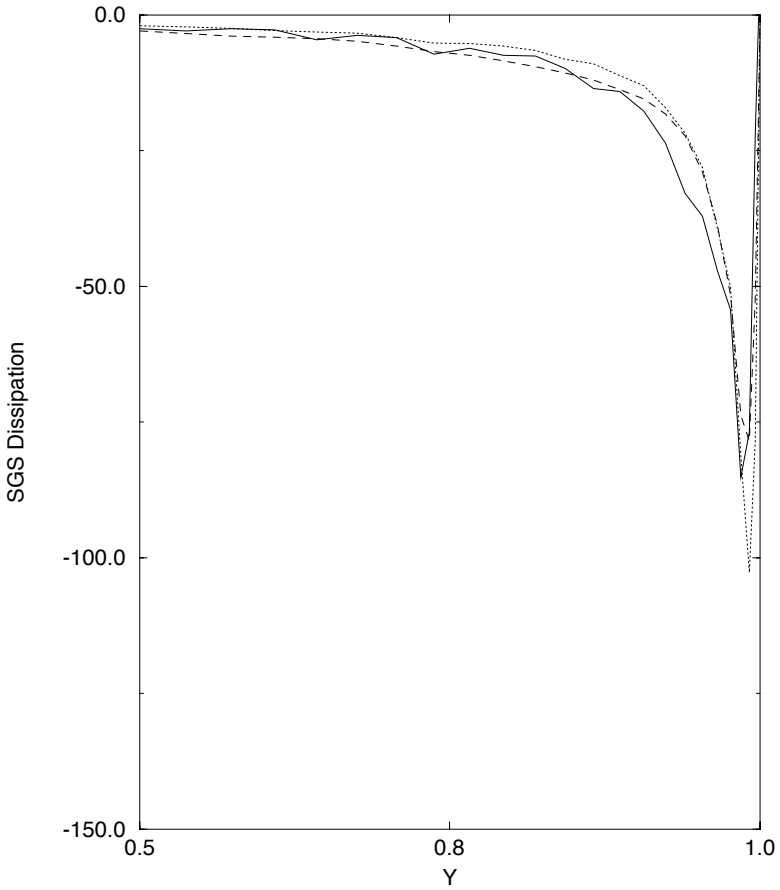

FIGURE 6. Subgrid-scale dissipation for the dynamic model and anistropic models. ——— : Dynamic model; ····· : Unclipped C=.25; - - - - : Clipped C=.075.

are 2 normalization constants needed to enforce (2). As a result, the stencil corresponding to the implementation of (5) involves 7 points in the first case and 27 in the second one. Figure 1 sketches the particular form of the stencil in the first case.

We have compared the results of LES on a 32^3 grid using the clipped anisotropic model (6), as well as the Smagorinsky model, with a 512^3 DNS. The coefficients of the various models have all been tuned to yield an energy decay which matches the DNS results (Fig. 2). The enstrophy decay curves in Fig. 3 show that the anisotropic models behave better than the Smagorinsky model up to time $T \sim 5$. This is confirmed by the energy spectra showed in Fig. 4. Past this time, all models are too dissipative in the high modes, with slightly better results for the anisotropic model (Fig. 5). The particular implementation chosen for the anisotropic model (isotropic vs tensor-product filter form) does not seem to significantly affect the results.

2.2.2 Channel calculations

This case is more challenging as it is well known that the Smagorinsky model is unable in this geometry to give good results in the absence of *ad hoc* damping at the walls or dynamic coefficient calculation.

We show comparisons between the anisotropic model and the so-called global

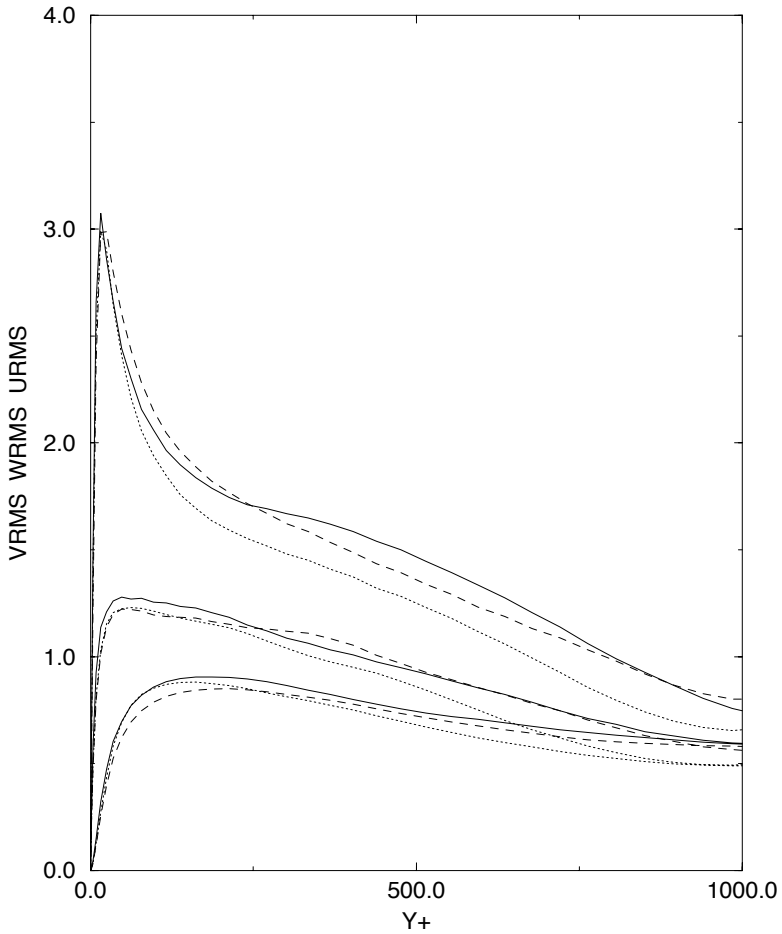

FIGURE 7. Turbulence intensities in wall coordinates; top curves: streamwise velocity, middle curves: normal velocity, bottom curves: spanwise velocity. Symbols same as Fig. 6.

dynamic model (Germano *et al.* 1991), which can considered as the best available model for this geometry. Our tests are done in the context of a Tchebytchev-Fourier collocation code (Kim *et al.* 1987). In this numerical scheme, the Crank-Nicolson time-advancing scheme is used for diffusion in the wall normal direction together with a third order Runge-Kutta method to advance the nonlinear convection and SGS terms. Periodic boundary conditions are assumed in the streamwise and spanwise directions and no-slip conditions at the walls located at $y = \pm 1$. Dealiasing is performed in the periodic directions, and the pressure is updated at each iteration to maintain a constant momentum throughout the calculation. We have focused on the case of a Reynolds number of $Re_\tau = 1,030$ based on the shear velocity, which corresponds to a Reynolds number of about $25,000$ based on the centerline velocity and the channel half-width.

The anistropic model has been implemented with the tensor-product filter ζ_2. Note that the grid refinement given by the Tchebytchev collocation points in the wall normal direction implies a variable eddy-viscosity length scale in this direction as explained in 2.1.2. Two cases have been considered: in the first one the method

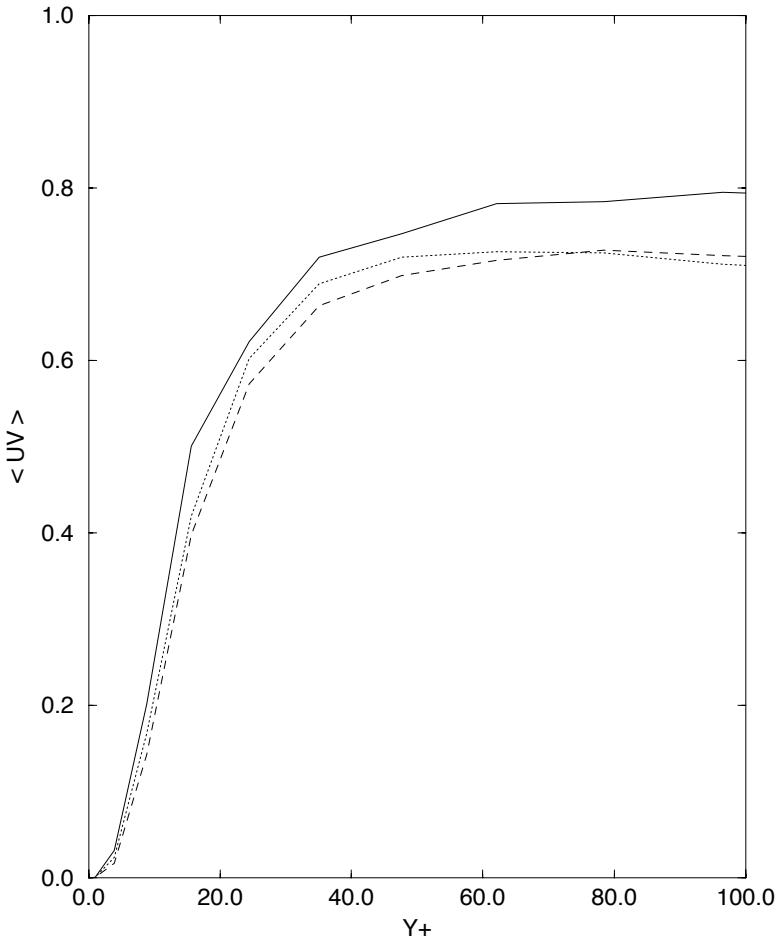

FIGURE 8. Large scale shear stress in wall coordinates. Symbls same as Fig. 6.

(5) is used without any clipping and a coefficient $C = 0.25$, while in the second a method similar to (6) is used in order to prevent the backscatter from overwhelming the molecular dissipation. In this latter case, a smaller value of the coefficient was chosen ($C = 0.075$). Figure 6 shows the subgrid-scale dissipation averaged on planes parallel to the walls. The similarity of the profiles obtained by the anisotropic models and the dynamic model is striking and confirms that the anisotropic model has a much better behavior in near wall regions than the Smagorinsky model. This observation is confirmed by the results obtained for the velocity fluctuations in Fig. 7 and the shear stresses in Fig. 8. We refer to (Cottet 1997) for more numerical results for this case.

3. Future plans

Tests of the anisotropic model have shown the superiority of this model over the Smagorinsky model. This superiority, which can be expected from the *a priori* tests that can be found in the literature, has been confirmed in LES using the present method. The efficacy of the model has gained from its ability to incorporate a truly anistropic backscatter control. The performance of the model both in isotropic and wall-bounded flows encourage trying it for other flows such as shear layers or jets.

Another direction of research is the implementation of a dynamic procedure to compute the model coefficient, along the lines suggested by Cottet (1997). On the basis of the present results, one can expect that this technique should not produce highly oscillatory values for the coefficient. In other words, the anisotropic model should be better conditioned than the Smagorinsky model for a dynamic procedure, in particular when no averaging over homogeneous directions can be used to stabilize it.

REFERENCES

COTTET, G. H. 1997 Anisotropic subgrid-scale models for Large Eddy Simulations of turbulent flows. *submitted.*

GERMANO, M., PIOMELLI, U., MOIN, P. & CABOT, W. H. 1991 A dynamic subgrid-scale eddy viscosity model. *Phys. Fluids A.* **3,** 1760-1765.

KIM, J., MOIN, P. &MOSER, R. 1987 Turbulence statistics in fully developed channel flow at low Reynolds number. *J. Fluid Mech.* **177,** 133-166.

LIU, S., MENEVEAU, C. & KATZ, J. 1994 The property of similarity subgrid-scale models. *J. Fluid Mech.* **275,** 83-119.

VREMAN, V., GEURTS, B. & KUERTEN, H. 1997 Large-eddy simulations of the turbulent mixing layer. *J. Fluid Mech.* **339,** 357-390.